中國機械工程學刊第四十一卷第五期第 565~573 頁(民國一百零九年)
Journal of the Chinese Society of Mechanical Engineers, Vol.41, No.5, pp 565~573(2020)

Effect of Etching Parameters on Gate Profile by Anisotropic Chemical Etching

Kun-Dar Li* and David Ta-Wei Lin **

Keywords：Crystallographic etching, Anisotropic chemical etching, Modeling, Gate profile

ABSTRACT

This pioneer study presents the phenomena of anisotropic chemical etching in the range of the linewidth 15nm~100nm. In this study, a phase-field model is established and a resist mask is appointed on the surface to simulate a chemical etching process with a gate geometry. In the numerical simulations, the isotropic and anisotropic etching conditions are both evaluated to explore the fine chemical etching circumstances. In addition, the influences of etching parameters, such as the etching rate and the strength of the anisotropy, on the characteristics of gate profile are also demonstrated. From the simulation results, it shows that a larger loss of linewidth or a higher etch bias is involved with the increase of the etching rate. While an anisotropic etching is considered, a faceted-etching profile would be generated and simultaneously the etch bias could be suppressed during the etching process. As the anisotropy is strengthened, the characteristic profile becomes more distinct with a less loss of the linewidth. These numerical simulations could provide a methodical guidance to concisely control the fine etching profile, and broaden the applications of chemical etching in the advanced robust manufacturing technologies.

INTRODUCTION

In consideration of etch directionality, the dry etching traditionally should be implemented as the linewidth is smaller than 3 μm but expensive cost. For the reason of unit price of MEMS product decreasing, wet etching is still worth and important in its improved research. Wet etching combined with optical technology will result in the advanced fabricated process. Kwon et al. (2020) reported that the laser-induced backside wet etching is an important manufacturing technology for fabricating high aspect ratio microfeatures of glass. Zhou et al. (2020) also noted that the UV irradiation-prompting wet etching is a promising technology of nano rod to nanotube. The nano-scale anisotropic wet etching mechanism begins to be noticed gradually as stated by Grinys et al. (2020). Sebastian et al. (2020) expressed the main target for the improvement of fabrication technology in the high-tech semiconductor industry are increase in performance, increase in reliability, reduction in cost, etc. In the manufacturing processes, a complicated sequence of chemical and physical operations is included in order to construct numerous structures and devices. Among various fabrication technologies, the etching technique play significant role to precisely generate the correct structures or patterns on the substrate surface, shown by Joubert et al. (2003) and Zrir et al. (2020). Without the accurate performance of etch, the device or chip will not function. Including the advantages of low cost, fast, precise, and reproducible process with simple equipment, Gosalvez et al. (2010) had demonstrated that wet chemical etching has good selectivity to the underlying film, and no risk of plasma damage to devices.

Regarding to the intrinsic properties of chemical etching, two basic etch profiles are involved, such as isotropic and anisotropic. When all crystallographic orientations of substrate materials are etched with the same rate, an isotropic etch profile would be gained. Owing to the undercutting of the etch-resistant mask during an isotropic etching, an undesirable loss of linewidth in the design patterns would be implicated. On the other hand, while the removal of atoms from the substrate is remarkably slow along certain lattice orientations, an anisotropic etching occurs. Sebastian et al. (2020) explored that in some circumstances, e.g., the patterning of nanodevices with small linewidths and features, the anisotropic etch is desired and crucial. Depending on the etching conditions, different type of etching profiles can be implemented and it provides important clues to tune the morphology of the etched surfaces with particular geometries. In addition to etch profile, affecting the etching performance etch rate is another key parameter in a chemical etching process.

Paper Received September, 2020. Revised October, 2020. Accepted October, 2020. Author for Correspondence: David T.W. Lin.
* *Professor, Department of Materials Science, National University of Tainan, Tainan 70005, Taiwan*
** *Professor, Department of Materials Science, National University of Tainan, Tainan 70005, Taiwan*

In general, controlled by the reactant concentration, temperature, etc., etch rate can be dramatically increased under a high temperature or high concentration circumstance. A rougher etched surface and a more isotropic etch profile usually tends to be formed with a fast etch rate. Hence, the formation of the etch profile or morphology is correlated to a complex process and manipulated by multiple factors, especially for the characteristic patterns with vertical structures or walls via a resist-mask etching.

Over the past decades, extensive researches had been performed towards understanding the mechanisms and variables involved in the chemical etching processes through the experimental and theoretical models, such as Grinys et al. (2020), Yu et al. (2017), Wang et al. (2006), Gosalvez et al. (2011), Rola et al. (2011), and Montoliu et al. (2013). Many fundamental issues had been addressed intendedly, such as linewidth control and morphological modification. In order to compensate the excessive materials below the resist-mask from undercutting, the common strategy is to oversize the resist mask features and carefully monitor the etch conditions to finish with a correct feature size and shape. All of these processes requires a detailed knowledge of the thermodynamics and kinetics in chemical etching reactions. In this study, a phase field model concerning atomic removal and diffusion on crystallography facets has been proposed to investigate the anisotropic chemical etching with characteristic gate profile. Various etching parameters are taken into consideration to demonstrate their influence on the profile formation and evolution during etching process. Furthermore, the quantitative measurements in terms of linewidth and etch bias are utilized to assess the etching procedures. For each set of parameters, a simulation is performed to obtain information about the predicted behavior of a specific etching condition, and the overall performance of etching process is then extracted from the set of simulation results. This study presents the numerical results on the primary mechanisms led to the final structures of gates after a chemical etching treatment. The etching behaviors, including the isotropic and anisotropic reactions, can be well explained and predicted. From this model and simulations, it would provide useful information to enhance the manufacturing technologies of anisotropic chemical etching, minimize the limits of linewidth and the pattern designs with complicated resist-mask during device processing in modern semiconductor industry.

EXPERIMENTAL

As well known, chemical etching is governed by thermodynamics and reaction kinetics. To investigate the issues related to the variations of the linewidth and surface profile in a gate etching, in this study a numerical method is applied to simulate a manufacturing process of a chemical etching. A theoretical model with a gate geometry is built, and the formation and evolution of the linewidth and the etch profile could be revealed numerically. Based on the phase field method with a field variable of the vacancy concentration in the matrix (c_v), Imada (1978), Asp and Agren (2006), and Li and Miao (2018) had separately proposed a comparable kinetic equation to describe the etching behavior, such as:

$$\frac{\partial c_v}{\partial t} = \varepsilon_{chem} \cdot |\nabla c_v|^2 + \nabla \cdot \left(\frac{M}{N^2} \nabla \left(\frac{\partial G}{\partial c_v} \right) \right), \qquad (1)$$

where t is the time, ε_{chem} is the vacancy production rate depending on the reactions between the matrix and the etchant in the chemical etching, M is a coefficient of atomic mobility, N is the number of atomic sites per unit volume, G is the free energy of the system. In Eq. (1), the first term of $|\nabla c_v|^2$ represents the etching phenomena happens at the interface of the material-vacancy system, while the second term in the right-hand side describes the diffusion of substrate atoms driven by the thermodynamic equilibrium. In a composition field, the low-level vacancy concentration represents the phase of the substrate, while the high-level vacancy concentration expresses the pseudo-phase of void. Owing to the chemical actions, the vacancies would be induced into the matrix to increase the vacancy concentration. By capturing the field variable of the vacancy concentration with time, the formation and evolution of etched profile during chemical etching process could be carved.

Tanaka et al. (2004), Gosalvez et al. (2006), and Hynninen et al. (2008) had proved that in general the chemical etching rate is crucially related to the crystallographic orientation. In order to describe a three-dimensional system, the spherical coordinate is employed in this study. The polar angle is expressed by $\Theta = \cos^{-1}\left(\frac{c_{v_z}}{|\nabla c_v|}\right)$ while the azimuthal angle is $\Phi = \tan^{-1}\left(\frac{c_{v_y}}{c_{v_x}}\right)$, where c_{v_x}, c_{v_y} and c_{v_z} are the partial differentiations of the field variable c_v with respect to the axes of x, y and z. Regarding to the anisotropic source term of vacancy production rate in Eq. (1), ε_{chem} is assumed as:

$$\varepsilon_{chem}(\Theta, \Phi) = \varepsilon_{ch}^0 \cdot [A(\Theta, \Phi)]^2, \qquad (2)$$

where ε_{ch}^0 is the average chemical etching rate, and $A(\Theta, \Phi)$ presents the chemical etching along the crystallographic orientation. For instance, $A(\Theta, \Phi) = 1$ represents an isotropic chemical etching condition. If a preferred etching orientation is taken place in a crystalline structure, according to Younsi and Cartalade (2016), different mathematical formula needs to be applied, such as:

$$A_{<100>}(\Theta,\Phi) = (1-3\eta)\left[1 + \frac{4\eta}{1-3\eta}(\sin^4\Theta\cdot(\sin^4(\Phi)+\cos^4(\Phi)) + \cos^4\Theta)\right], \quad (3)$$

where $A_{<100>}(\Theta,\Phi)$ represents the preferred etching orientation along $<100>$ directions. η is the strength of anisotropy of the etching rate, which is affected by the etchant, concentration, temperature, etc. While other preferred etching orientations is considered, a proper form of $A(\Theta,\Phi)$ can be used to simulate a corresponding condition by this model.

In addition, for a crystalline matrix anisotropic interfacial energy should also be included in the system free energy (G). In the past decades, the system free energy with anisotropic interfacial energy was well investigated by Eggleston et al. (2001) and Kobayashi (1993), and expressed as:

$$G = \int_V \left[g(c_v) + \frac{\gamma^2}{2}|\nabla c_v|^2\right] dV, \quad (4)$$

where $g(c_v)$ is the local free energy of the system, γ is a gradient coefficient related to the interfacial energy. The local free energy of $g(c_v)$ is taken a form of double well energy landscape, such as the regular solution formula $g(c_v) = Nk_BT[c_v \ln c_v + (1-c_v)\ln c_v] + N\Omega c_v(1-c_v)$ adopted by Asp and Agren (2006), where k_B is the Boltzmann's constant, T is the absolute temperature, and Ω represents the interactions between vacancies and atoms. For an isotropic or amorphous interface, γ could be treated as a constant. Otherwise, γ should be taken as a function of the local unit normal vector to present the anisotropy in the interfacial region for the anisotropic or crystalline interface. In a cubic system, a similar expression of $\gamma(\Theta,\Phi)$ is given by Kim (2007) as:

$$\gamma(\Theta,\Phi) = \gamma_0(1-3\lambda)\left[1 + \frac{4\lambda}{1-3\lambda}(\sin^4\Theta\cdot(\sin^4(\Phi)+\cos^4(\Phi)) + \cos^4\Theta)\right], \quad (5)$$

where γ_0 is the average interfacial energy and λ is the strength of anisotropy of the interfacial energy. With a proper treatment of the interfacial energy, a crystalline substrate could be readily depicted during chemical etching process. In addition, the anisotropic mobility of $M(\Theta,\Phi)$ for a cubic structure can then be written as:

$$M(\Theta,\Phi) = M_0(1-3\lambda)^{-2}\left[1 + \frac{4\lambda}{1-3\lambda}(\sin^4\Theta\cdot(\sin^4(\Phi)+\cos^4(\Phi)) + \cos^4\Theta)\right]^{-2}, \quad (6)$$

where M_0 is the average mobility of atoms.

Combining Eqs. (2), (3), (4), (5) and (6) into Eq. (1), an anisotropic phase field model could be given as:

$$\frac{\partial c_v}{\partial t} = \varepsilon_{chem}(\Theta,\Phi)\cdot|\nabla c_v|^2 + \nabla\cdot\left(\frac{M(\Theta,\Phi)}{N^2}\nabla\left(\frac{\partial g(c_v)}{\partial c_v} - \nabla\cdot(\gamma(\Theta,\Phi)^2\nabla c_v) - \partial_x\left(\gamma(\Theta,\Phi)\cot\Theta\frac{\partial\gamma(\Theta,\Phi)}{\partial\Theta}\frac{\partial c_v}{\partial x} - \gamma(\Theta,\Phi)\csc^2\Theta\frac{\partial\gamma(\Theta,\Phi)}{\partial\Phi}\frac{\partial c_v}{\partial y}\right) - \partial_y\left(\gamma(\Theta,\Phi)\csc^2\Theta\frac{\partial\gamma(\Theta,\Phi)}{\partial\Phi}\frac{\partial c_v}{\partial x} + \gamma(\Theta,\Phi)\cot\Theta\frac{\partial\gamma(\Theta,\Phi)}{\partial\Theta}\frac{\partial c_v}{\partial y}\right) + \partial_z\left(\gamma(\Theta,\Phi)\tan\Theta\frac{\partial\gamma(\Theta,\Phi)}{\partial\Phi}\frac{\partial c_v}{\partial z}\right)\right)\right). \quad (7)$$

To perform the numerical simulations, a length scale (l_0) and time scale (τ) are used to normalize the kinetic equation of Eq. (7) for a chemical etching process. The length scale of l_0 and the time scale are defined by $l_0 = \gamma_0\cdot(Nk_BT)^{-1/2}$ and $\tau = (\gamma_0/k_BT)^2/M_0$, respectively. Therefore, a dimensionless equation of Eq. (7) is further presented as:

$$\frac{\partial c_v}{\partial t^*} = \varepsilon^*_{chem}(\Theta,\Phi)\cdot|\nabla^* c_v|^2 + \nabla^*\cdot\left(M^*(\Theta,\Phi)\nabla^*\left(\frac{\partial g^*(c_v)}{\partial c_v} - \nabla^*\cdot(\gamma^*(\Theta,\Phi)^2\nabla^* c_v) - \partial_{x^*}\left(\gamma^*(\Theta,\Phi)\cot\Theta\frac{\partial\gamma^*(\Theta,\Phi)}{\partial\Theta}\frac{\partial c_v}{\partial x^*} - \gamma^*(\Theta,\Phi)\csc^2\Theta\frac{\partial\gamma^*(\Theta,\Phi)}{\partial\Phi}\frac{\partial c_v}{\partial y^*}\right) - \partial_{y^*}\left(\gamma^*(\Theta,\Phi)\csc^2\Theta\frac{\partial\gamma^*(\Theta,\Phi)}{\partial\Phi}\frac{\partial c_v}{\partial x^*} + \gamma^*(\Theta,\Phi)\cot\Theta\frac{\partial\gamma^*(\Theta,\Phi)}{\partial\Theta}\frac{\partial c_v}{\partial y^*}\right) + \partial_{z^*}\left(\gamma^*(\Theta,\Phi)\tan\Theta\frac{\partial\gamma^*(\Theta,\Phi)}{\partial\Phi}\frac{\partial c_v}{\partial z^*}\right)\right)\right), \quad (8)$$

where t^* is the normalized time, $\varepsilon^*_{chem}(\Theta,\Phi) = \frac{\varepsilon_{chem}(\Theta,\Phi)}{{l_0}^2}\cdot\tau$, $x^* = x/l_0$, $y^* = y/l_0$, $z^* = z/l_0$, $\nabla^* = l_0\nabla$, $M^*(\Theta,\Phi) = M(\Theta,\Phi)/M_0$, $g^*(c_v) = g(c_v)/Nk_BT$, and $\gamma^*(\Theta,\Phi) = \gamma(\Theta,\Phi)/\gamma_0$.

In the numerical simulations, the finite volume method proposed by Vinokur (1989) is utilized to solve the partial differential equation of Eq. (8). In order to create a three-dimensional geometric model, a mesh size of $60\times60\times30$ with grid spacing of 0.5 is employed. Periodical boundary conditions are used in the *x* and *y* axes, while zero flux are set at $z = 0$ and $z = L_z$ where L_z is the size of the mesh in the z direction for the boundary conditions. A high vacancy concentration in the interval of $[0.9, 1.0]$ is set in the top face of the model to denote the free surface of substrate. For the matrix, an initial value of vacancy concentration in the interval of $[0, 0.1]$ is assigned arbitrarily to imitate the intrinsic vacancies. In addition, a mask pattern is established in the center

of the top face with a size of 60×30 to mimic a gate profile etching process. A series of the numerical simulations with time step of 0.5 are implemented to investigate the formation and evolution of surface morphologies during a chemical etching. Based on the relevant literatures of Li and Miao (2018), Yu and Lu (2005), and Suo and Lu (2000), the physical parameters for the numerical calculation are employed as $N\sim1\times10^{19}m^{-2}$, ${\gamma_0}^2\sim8\times10^{-19}J$, $\lambda\sim0.06$, and $\Omega/k_BT\sim3.75$. According to these parameters, the length scale is calculated as ~4.25nm in this study. Other experiment-related parameters, e.g., the chemical etching rate and the atomic mobility, are estimated by the preliminary calculations to acquire the rational values. Furthermore, these experiment-related parameters are methodically changed to evaluate their effects on the morphological evolution during a gate profile formation by anisotropic chemical etching. Based on the simulation results, the linewidth of the gate and the etch bias during the etching process are also measured to quantitatively analyze the simulations. Etch bias is a measure of the change in the linewidth or space of a critical dimension after performing an etch process. It is usually caused by undercutting, but can also be the result of an etch profile. Etch bias for the linewidth change is measured by comparing pre-etch linewidth in resist-mask with post-etch linewidth of the same feature. The detailed definition of etch bias can be referred to Quirk and Serda (2011). In accordance with these numerical simulations, the influence of etching parameters on the formation of surface morphology and gate profile could be demonstrated distinctly.

RESULTS & DISCUSSION

In Fig. 1, an isotropic chemical etching is firstly considered and the evolution of etching profile is numerically reconstructed by solving the partial differential equation of Eq. (8). In this case, the etching rate of ε^*_{chem} is taken as 0.01 and the strength of anisotropy is assumed as 0 to represent an isotropic etching. From Fig. 1, it could be seen that in the initial stage of etching process the etching reaction starts at the surface area without resist-mask. The linewidth of the gate could be easily identified, as shown in Fig. 1a at $t^*=50$. While the chemical etching is proceeded, the exposed substrate is gently etched out and the variations of surface depths between etched and protected areas are revealed, as demonstrated in Fig. 1b, c. At this time, some fluctuations on the etched surface could also be observed. This temporary profile is mainly caused by the kinetic etching reaction and the atomic diffusion in a crystalline substrate. It should also be noticed that a deeper etching spot could be found in the edges between the resist mask and exposed substrate. It is speculated that due to an isotropic etching the etching reaction happens not only at the exposed surface, but also the sidewall underneath the mask. Therefore, a high vacancy concentration is accumulated at the edge of the pattern boundary. After a certain etching time, the bumpy surface would be vanished and a smoothened surface profile could be gradually evolved, as shown in Fig. 1d, e. Consequently, a decreased linewidth of the gate is disclosed in these figures. In addition, a small trench near the edges of the gate could still be seen. While a stable condition is established, a characteristic profile with similar contour would be retained. Until the last stage of etching process, a smooth surface profile around the edges of the resist mask is distinctly demonstrated, as displayed in Fig. 1f. These featured surfaces and the profile evolution are fitted well with the experimental observations of the undercutting phenomena and the etch bias in a chemical etching process conducted by Quirk and Serda (2011), Sebastian et al. (2020), and Zrir et al. (2020). This numerical model has provided an efficient method to investigate the related issues of the gate profile formation by chemical etching.

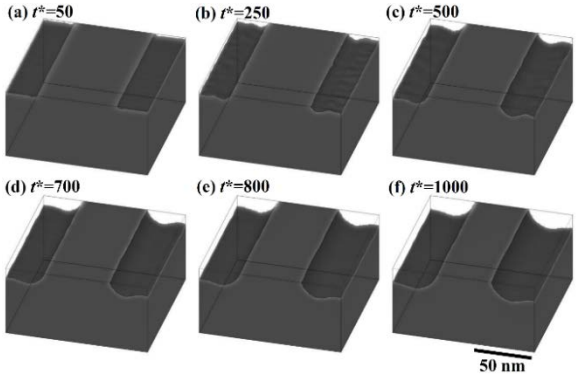

Fig. 1 The numerical simulation for the formation and evolution of gate profile during isotropic chemical etching

In order to demonstrate the influence of etching rate on the profile evolution, a higher etching rate with $\varepsilon^*_{chem}=0.02$ is taken into consideration while other numerical parameters are kept the same as those used in Fig. 1. Fig. 2 presents a simulation result of surface profile formation and evolution for an isotropic chemical etching with a high etching rate. As shown in Fig. 2a, a nearly identical profile evolution is observed in the early stage of etching reaction for a high etching rate condition, and the gate profile is perceptibly revealed on the substrate surface. While the reaction time is increased, the unprotected surface moves downward with ripple-like morphology, as shown in Fig. 2b, c. Since a high etching rate is considered, the downward migration rate of the etched surface is accelerated. In addition, owing to the effect of the undercutting at the mask edges the linewidth of the gate is reduced significantly with a broadened etched-area, as shown in Fig. 2d, e, f. In the late stage of etching process, a smooth surface morphology with a deep and wide profile could be seen. From the

numerical simulation, there is only about $1/5$ linewidth of the gate remained while the etching rate of ε^*_{chem} is doubled, as presented in Fig. 2f.

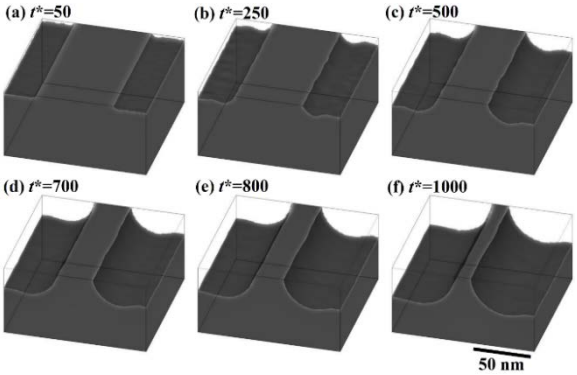

Fig. 2 The numerical simulation for the formation and evolution of gate profile during isotropic chemical etching with high etching rate

To demonstrate the characteristics of surface profile in Fig. 1 and 2 more clearly, the quantitative linewidth of the gate and the etch bias during the etching process are illustrated in Fig. 3a, b, respectively. From Fig. 3a, it can be seen that the linewidth of the gate is reduced with the increased etching time. In addition, the etching rate has a great influence on the linewidth of the gate. For the case of a low etching rate, the linewidth of the gate is decreased from $\sim$70 nm to $\sim$46 nm, while the linewidth is only about 12nm in the late stage of a high etching rate.

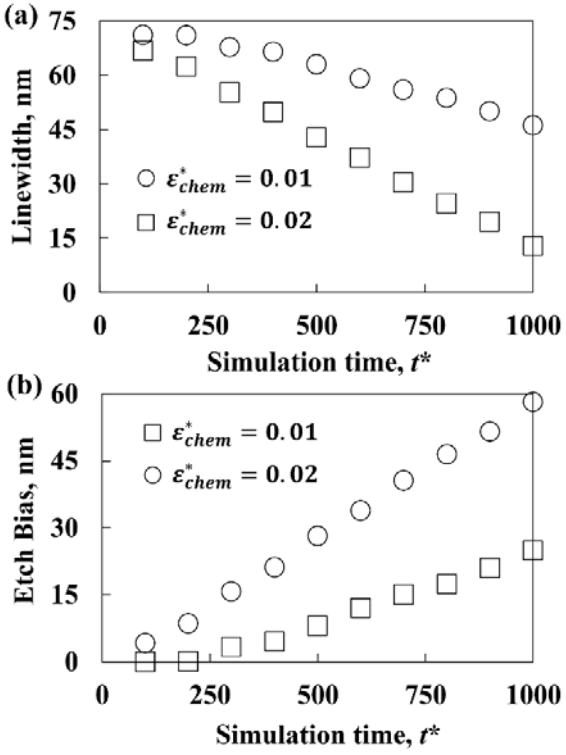

Fig. 3 The quantitative analyses of the numerical simulations during isotropic chemical etching with different etching rate, (a) the linewidth of the gate, and (b) the etch bias.

The effect of undercutting had been amplified under a high etching rate condition. Based on Fig. 3b, the etch bias is generally increased with the etching process. Furthermore, a high etch bias is involved while the etching rate is raised. From the numerical results, the etch bias is increased about 2.3 times with a doubled etching rate (ε^*_{chem} from 0.01 to 0.02). The quantitative analyses in Fig. 3a, b distinctly demonstrate the influence of etching rate on the etching profile and the undercutting during the chemical etching process.

In the next case, an anisotropic chemical etching with $< 100 >$ preferred-orientation is considered to imitate an etching process in a crystalline substrate. The simulation result of the formation and evolution for the etched profile is presented in Fig. 4.

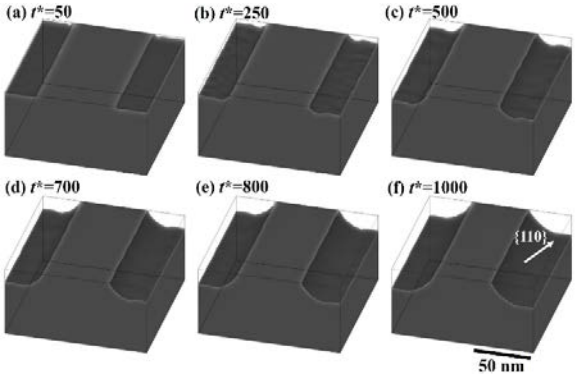

Fig. 4 The numerical simulation for the formation and evolution of gate profile during anisotropic chemical etching.

In this case, the strength of anisotropy (η) in Eq. (3) is taken as 0.18, while the etching rate of $\varepsilon^*_{chem} = 0.01$ with the same other numerical parameters used in Fig. 1 are employed. From Fig. 4a, b, c, it could be found that in the early state of etching process there is no significant difference on the profile evolution between isotropic and anisotropic etching, by comparing to Fig. 1a, b, c. The main surface feature is small ripples formed in the etched surface with a deeper trench along the edges of the resist mask. After a certain amount of etching time, a characteristic profile is gradually emerged in the anisotropic etching along $< 100 >$ preferred-orientation. A faceted surface profile could be seen at the edges of the resist mask in Fig. 4d, e, which is different to the smooth surface morphologies in the isotropic etching in Fig. 1d, e, f. In Fig. 4f, the faceted surface at the edges of the resist mask belong to $\{110\}$ planes. Additionally, from the difference of the gate linewidth between Fig. 4a, f, the effect of undercutting on the surface profile is

demonstrated plainly for the anisotropic chemical etching. To quantitatively illustrate the characteristics of surface structures for different conditions, Fig. 5 displays the linewidths and etch biases of the gate profiles during etching processes, including isotropic and anisotropic chemical etching. From Fig. 5a, it could be found that in the early stage the variations of the linewidths for different conditions are identical. Only a small difference appears at the late stage. In the anisotropic etching, a larger linewidth is obtained, and that could be attributed to the behavior of preferred-orientation etching. Major etching reaction happens at the certain crystallographic directions. Consequentially, a smaller etch bias is acquired for anisotropic etching, as shown in Fig. 5b.

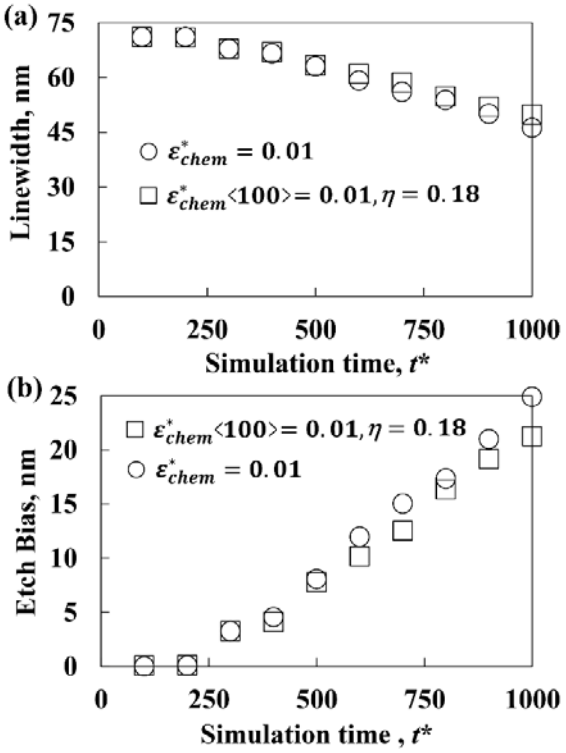

Fig. 5 The quantitative analyses of the numerical simulations during isotropic and anisotropic chemical etching, (a) the linewidth of the gate, and (b) the etch bias.

From the simulation results in Fig. 4 and 5, it proves that the anisotropic etching condition has a great influence on the gate profile. The behaviors of the anisotropic etching are affected by many factors, such as the preferred-orientation of the etching, and the strength of the anisotropy. To investigate the influence of these experimental factors on the gate profile, in this study various anisotropic etching conditions are further examined. At first different strengths of anisotropy in Eq. (3) are taken into consideration, such as $\eta = 0.3$ and 0.8, while other parameters are kept the same as used in Fig. 4. The formation and evolution of the gate profile during anisotropic etching for these conditions are demonstrated in Fig. 6 and 7, respectively.

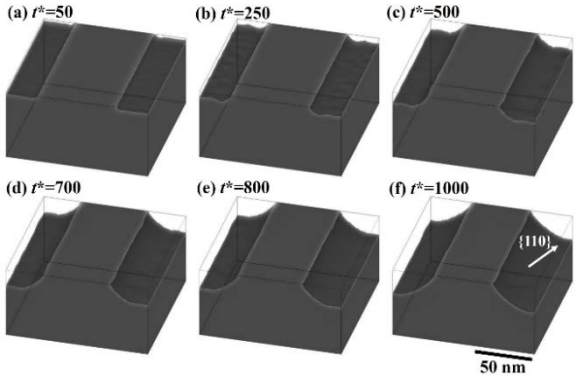

Fig. 6 The numerical simulation for the formation and evolution of gate profile during anisotropic chemical etching with anisotropic strength of η =0.3.

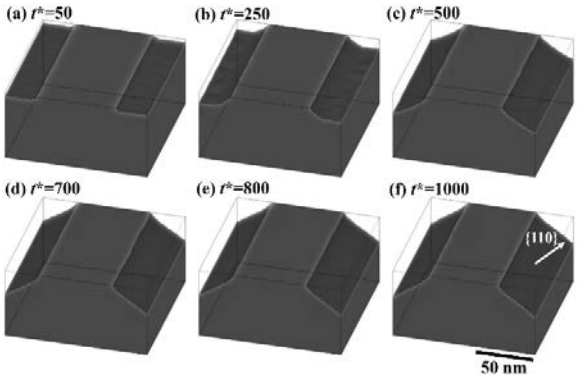

Fig. 7 The numerical simulation for the formation and evolution of gate profile during anisotropic chemical etching with anisotropic strength of η =0.8.

Under a high etching anisotropy, it is observed that without the protection of resist mask, an etched surface with small ripples would be formed, as shown in Fig. 6a, b, and Fig. 7a, b. While the etching time is increased, as demonstrated in Fig. 7c, the faceted {110} planes become more clear at the edges of the resist mask under a high strength of the anisotropy, comparing to Fig. 5c or Fig. 6c. In addition, with the increase of the anisotropic strength, the formation of the characteristic planes of {110} would be accelerated during the etching process, which could be found by a comparison of Fig. 6d, e, f and Fig. 7d, e, f. Not only the surface profile, but also the linewidth and etch bias of the gate could be altered due to the variation of the anisotropic strength. From the quantitative analyses of the linewidth and etch bias in Fig. 8a, b, the curves depicting the variations of the linewidth and etch bias in relative low strengths of anisotropy, such as $\eta = 0.18$ and 0.3, are almost overlapped. However, while the strength of anisotropy is increased to 0.8, a distinct difference of the linewidth and etch bias could be observed in the late stage of the etching process. A wider linewidth and a

less etch bias could be obtained with the increase of the anisotropic strength. At the simulation time of $t = 1000$, the etch bias for $\eta = 0.8$ is reduced up to 50% than that in $\eta = 0.18$. It also affirms that the strength of the anisotropy makes the preferred-planes of $\{110\}$ more distinct, and reduces the undercutting effect to decrease the etch bias.

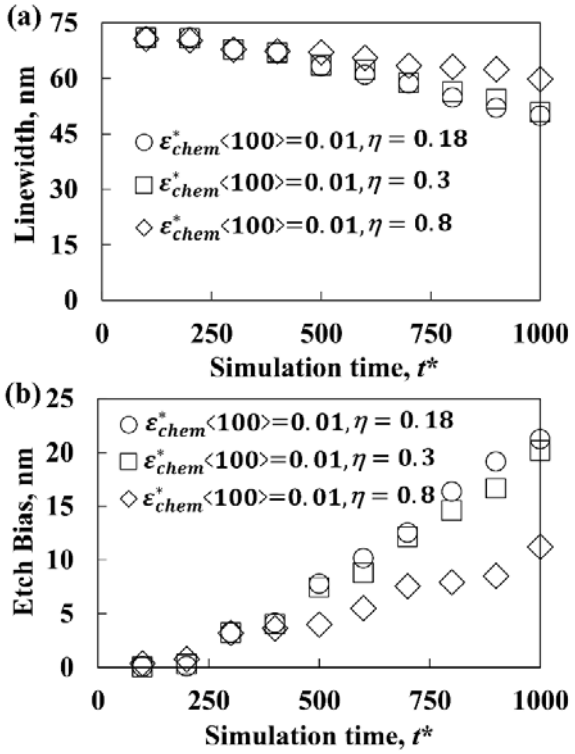

Fig. 8 The quantitative analyses of the numerical simulations during anisotropic chemical etching with different strengths of anisotropy, (a) the linewidth of the gate, and (b) the etch bias.

In the last case, the situation of the high etching rate with different strengths of the anisotropy is investigated to reflect these two factors simultaneously during surface profile formation in an anisotropic etching. Fig. 9, Fig. 10 and Fig. 11 demonstrate the numerical simulations of the evolution of gate profile with a high etching rate of $\varepsilon^*_{chem} = 0.02$, while $\eta = 0.18$, 0.3 and 0.8, respectively. Corresponding to the results in the isotropic etching of Fig. 2, the rate of surface evolution in Fig. 9 with a high etching rate becomes faster than that in Fig. 4 for the anisotropic etching. Comparing Fig. 2a, b, c, d, e, f with Fig. 9a, b, c, d, e, f, it is observed that the round profile along the edge of the resist mask is replaced by the faceted$-\{110\}$ planes in the anisotropic etching with high etching rate. While the strength of the anisotropy is increased, the faceted$-\{110\}$ planes would be formed earlier and the faceted features become more distinct, as shown in Fig. 9b, c, Fig. 10b, c, and Fig. 11b, c. In addition, it is found that the reductions of the linewidth of the gates are decreased with the increase of the anisotropic strength in a comparison of Fig. 9f, Fig. 10f, and Fig. 11f.

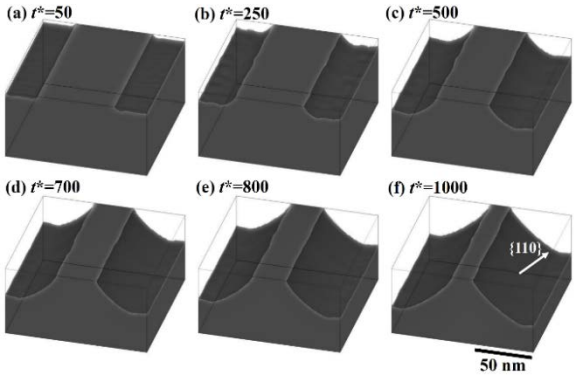

Fig. 9 The numerical simulation for the formation and evolution of gate profile during anisotropic chemical etching with high etching rate of ε^*_{chem}=0.02 and the anisotropic strength of η =0.18.

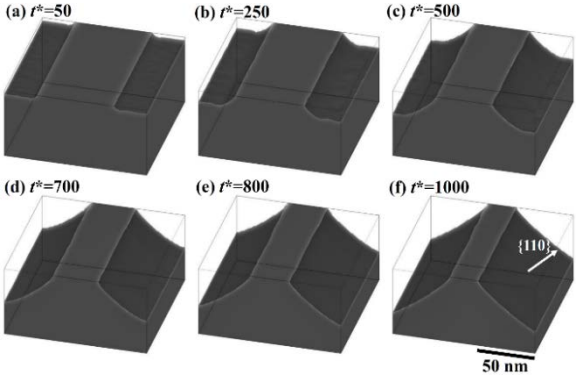

Fig. 10 The numerical simulation for the formation and evolution of gate profile during anisotropic chemical etching with high etching rate of ε^*_{chem}=0.02 and the anisotropic strength of η =0.3.

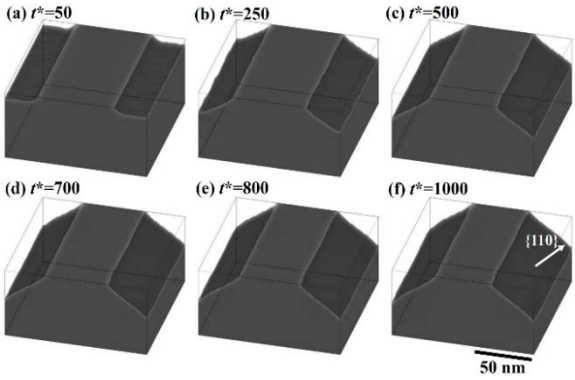

Fig. 11 The numerical simulation for the formation and evolution of gate profile during anisotropic chemical etching with high etching rate of ε^*_{chem}=0.02 and the anisotropic strength of η =0.8.

The identical results from the quantitative measurement based on the surface profile are displayed in Fig. 12. From Fig. 12a, b, it could be noticed that while the

strength of the anisotropy is changed from 0.18 to 0.8, the reduction ratio of the linewidth is varied from 70% to 30%, as the etch bias is altered from 50nm to 15nm that is reduced by ~1/3 times. According to these qualitative and quantitative analyses, the influence of the anisotropic strength on the surface profile becomes distinct under the high etching rate. The increased strength of the anisotropy enhances the formation of the faceted −{110} planes, and simultaneously reduces the effect of the undercutting and the etch bias.

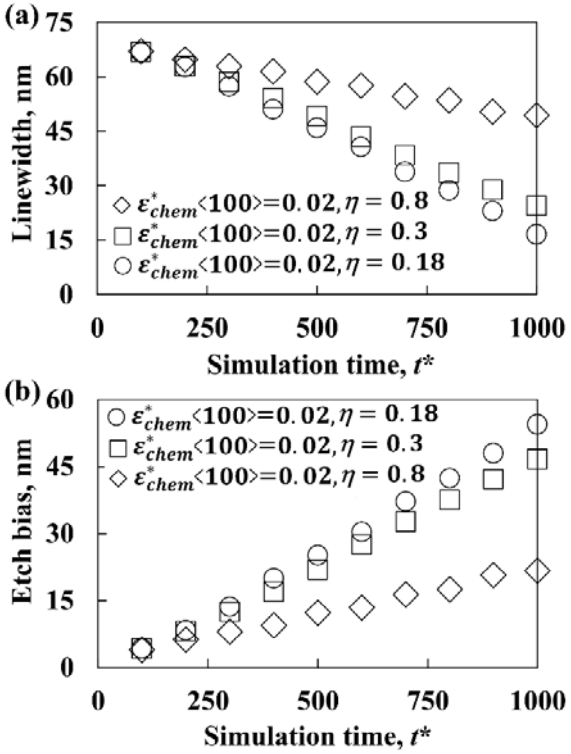

Fig. 12 The quantitative analyses of the numerical simulations during anisotropic chemical etching with high etching rate and different strengths of anisotropy, (a) the linewidth of the gate, and (b) the etch bias.

CONCLUSION

In summary, a numerical model based on the phase-field method is developed to simulate the evolution of gate profile during chemical etching process. In this study, the effect of undercutting on the profile formation is investigated theoretically under isotropic and anisotropic etching conditions. For an isotropic etching with a high etching rate, the effect of undercutting at the edge of the resist mask exert a significant influence on the surface characteristics to create the lowest linewidth and largest etch bias after the etching process. The reactions and behaviors could be emphasized with the increase of the etching rate; no matter an isotropic or anisotropic etching is considered. Oppositely, while the factor of the anisotropic etching is strengthened, the effect of undercutting could be obviously suppressed to induce the reduction of the etch bias and the retention of the linewidth of the gate profile. Furthermore, the features of faceted surface morphologies along crystallographic planes appear under anisotropic etching. These numerical simulations are consistent with the experimental observations. This theoretical model has well improved the understanding of the underlying mechanisms of chemical etching for gate profile with resist-mask. In addition, the influence of the etching parameters on the etching behaviors have been demonstrated systematically to enhance the modern manufacturing technology by the anisotropic chemical etching for the development of advanced materials.

ACKNOWLEDGMENTS

This work is supported by Ministry of Science and Technology, Republic of China (Taiwan) under grant MOST 106-2221-E-024-008-MY3.

REFERENCES

Asp, K. and Agren, J., “Phase-field Simulation of Sintering and Related Phenomena-A Vacancy Diffusion Approach,”; Acta Mater., Vol. 54, No. 5 pp. 1241-1248(2006).

Eggleston, J.J., McFadden, G.B., Voorhees, P.W., “A Phase-field Model for Highly Anisotropic Interfacial Energy,”; Physica D: Nonlinear Phenomena, Vol. 150, No. 1-2, pp. 91-103(2001).

Gosalvez, M.A., Cheng, D., Nieminen, R.M., Sato, K., “Apparent Activation Energy During Surface Evolution by Step Formation and Flow,”; New J. Phys., Vol. 8, pp. 269(2006).

Gosalvez, M.A., Zubel, I., Viinikka, E., Wet Etching of Silicon. In: Lindroos, V., Tilli, M., Lehto, A., Motooka, T. (Eds.), Handbook of Silicon Based MEMS Materials and Technologies. Elsevier Inc. William Andrew Publishing, Boston, pp. 375-407(2010).

Gosalvez, M.A., Pal, P., Ferrando, N., Hida, H., Sato, K., “Experimental Procurement of the Complete 3D Etch Rate Distribution of Si in Anisotropic Etchants Based on Vertically Micromachined Wagon Wheel Samples,”; J. Micromech. Microeng., Vol. 21, No. 12: 125007(2011).

Grinys, T., Drunga, T., Dobrovolskas, D., Dargis, R., Clark, A., “Wet Etching Mechanism of Er_2O_3 Grown on Si by Molecular Beam Epitaxy,”; Appl. Surf. Sci., Vol. 505:144452(2020).

Hynninen, T., Foster, A.S., Gosalvez, M.A., Sato, K., Nieminen, R.M., “Adsorption of Metal Impurities on H-terminated Si Surfaces and Their Influence on the Wet Chemical Etching of Si,”; J. Phys.: Condens. Matter., Vol. 20, No. 48:485005(2008).

Imada, M., “Void Lattice Formation-spinodal Decomposition of Vacancies,”; J. Phys. Soc. Jap.,

Vol. 45, pp. 1443-1448(1978).
Joubert, O., Pargon, E., Foucher, J., Detter, X., Cunge, G., Vallier, L., "Nanometer Scale Linewidth Control During Etching of Polysilicon Gates in High-density Plasmas,"; Microelectron. Eng., Vol. 69, No. 2-4, pp. 350-357(2003).
Kim, J., "Three-dimensional Numerical Simulations of a Phase-field Model for Anisotropic Interfacial Energy,"; Commun. Korean Math. Soc., Vol. 22, No.3, pp. 453-464(2007).
Kobayashi, R., "Modeling and Numerical Simulations of Dendritic Crystal Growth,"; Physica D: Nonlinear Phenomena, Vol. 63, No. 3-4, pp. 410-423(1993).
Kwon, K., Kim, H., Kim, T., Chu, C., "High Aspect Ratio Channel Fabrication with Near-infrared Laser-induced Backside Wet Etching,"; J. Materials Processing Tech., Vol. 278:116505(2020).
Li, K.D. and Miao, J.R., "Modeling the Characteristic Etch Morphologies Along Specific Crystallographic Orientations by Anisotropic Chemical Etching,"; AIP Advances, Vol. 8:025214(2018).
Montoliu, C., Ferrando, N., Gosalvez, M.A., Cerda, J., Colom, R.J., "Inplementation and Evaluation of the Level Set Method: Towards Efficient and Accurate Simulation of Wet Etching for Microengineering Applications,"; Comput. Phys. Commun., Vol. 184, No. 10, pp. 2299-2309(2013).
Quirk, M. and Serda, J., Semiconductor Manufacturing Technology, Pearson Education Taiwan Ltd., Taiwan (2011).
Rola, K.P. and Zubel, I., "Investigation of Si (*h k l*) Surfaces Etched in KOH Solutions Saturated with Tertiary-butyl Alcohol,"; J. Micromech. Microeng., Vol. 21, No.11:115026(2011).
Sebastian, E.M., Jain, S.K., Purohit, R., Dhakad, S.K., Rana, R.S., "Nanolithography and Its Current Advancements,"; Materials Today: Proceedings, Vol. 26, pp. 2351-2356(2020).
Suo, Z. and Lu, W., "Forces that Drive Nanoscale Self-Assembly on Solid Surfaces,"; J. Nanopart. Res., Vol. 2, No. 4, pp. 333-344(2000).
Tanaka, H., Yamashita, S., Abe, Y., Shikida, M., Sato, K., "Fast Etching of Silicon with a Smooth Surface in High Temperature Ranges Near the Boiling Point of KOH Solution,"; Sens. Actuators A: Phys., Vol. 114, No. 2, pp. 516-520(2004).
Vinokur, M., "An Analysis of Finite-difference and Finite-volume Formulations of Conservation Laws,"; J. of Comput. Phys., Vol. 81, No. 1, pp. 1-52(1989).
Wang, J., Guo, L.W., Jia, H.Q., Xing, Z.G., Wang, Y., Yan, J.F., Yu, N.S., Chen, H., Zhou, J.M., "Investigation of Characteristics of Laterally Overgrown GaN on Striped Sapphire Substrates Patterned by Wet Chemical Etching,"; J. Cryst. Growth, Vol. 290, pp. 398-404(2006).
Younsi, A. and Cartalade, A., "On Anisotropy Function in Crystal Growth Simulations Using Lattice Boltzmann Equation,"; J. Comput. Phys., Vol. 325, pp. 1-21(2016).
Yu, F., Yao, S., Römer, F., Witzigmann, B., Schimpke, T., Strassburg, M., Bakin, A., Schumacher, H.W., Peiner, E., Wasisto, H.S., Waag, A., "GaN Nanowire Arrays with Nonpolar Sidewalks for Vertically Integrated Filed-effect Transistors,"; Nanotechnology, Vol. 28, No. 9:095206(2017).
Yu, H. and Lu, W., "Dynamics of the Self-assembly of Nanovoids and Naunobubbbles in Solids,"; Acta Mater., Vol. 53, pp. 1799-1807(2005).
Zhou, F., Jing, W., Mao, Q., Liu, S., Xu, Y., Han, F., Wei, Z., Jiang, Z., "UV Irradiation-promoted Wet Etching of ZnO Nanorods to Nanotubes,"; Micro & Nano Letters, Vol. 15, No. 2, pp. 96-100(2020).
Zrir, M.A., Kakhia, M., AlKafri, N., "Forming Si Nanocrystals on Insulator by Wet Anisotropic Etching,"; Thin Solid Films, Vol. 696:137766(2020).

異向性化學蝕刻參數對閘極輪廓影響之研究

李昆達　林大偉
國立臺南大學材料科學系

摘要

本研究前瞻地提出當線寬在15nm~100nm範圍內之異向性化學蝕刻現象研究。於本研究中，以相場模型建立基材表面上具有線幾何設計之光阻圖樣以進一步模擬閘極化學蝕刻製程。為了更詳盡探討化學蝕刻環境之影響，本研究比較等向性與異向性不同之蝕刻條件。此外，對閘極輪廓特性有決定性之影響因素，如蝕刻速率與異向性強度等，也一併深入探究。模擬結果發現，隨著蝕刻速率的提高，會產生較大的蝕刻偏差。但異向性蝕刻因產生多面向蝕刻之影響，將可抑制此過度的蝕刻偏差。而增強異向性蝕刻之強度，其閘極輪廓將因線寬損失的降低而更為清晰。本研究所提出之方法將可為化學蝕刻提供製程參數之設計規則，以便能更精細的控制化學蝕刻形貌與輪廓，並進一步擴展了化學蝕刻之應用範圍。